Quantitative and rapid detection of nanoplastics labeled by luminescent metal phenolic networks using surface enhanced Raman scattering

*Haoxin Ye[a], Guang Gao[b], Tianxi Yang[a]**

a Food, Nutrition and Health Program, Faculty of Land and Food Systems, The University of British Columbia, Vancouver V6T1Z4, Canada

b Life Sciences Institute, The University of British Columbia, Vancouver V6T1Z2, Canada.

Corresponding author: Tianxi Yang (tianxi.yang@ubc.ca)

Keywords: Plastic contaminant; Rapid analysis; Accurate quantification; SERS; L-MPNs labeling

ABSTRACT

The rising incidence of nanoplastics contamination in environmental ecosystems has led to substantial health risks. Traditional analysis methods are suboptimal due to their inability to efficiently analyze nanoplastics at low concentrations and time-consuming operations. Herein, we developed an innovative strategy, employing luminescent metal–phenolic networks (L-MPNs) coupled with surface-enhanced Raman spectroscopy (SERS) to separate and label nanoplastics, thus facilitating rapid, sensitive and quantitative detection of nanoplastics. We used L-MPNs composed of zirconium ions, tannic acid and rhodamine B, to uniformly label diverse sizes (50-500 nm) and types of nanoplastics (i.e., polystyrene, polymethyl methacrylate, polylactic acid). Rhodamine B, serving as a Raman reporter in L-MPNs-based SERS tags can offer sufficient sensitivity for trace measurement of nanoplastics and L-MPNs labeling can also facilitate separation of nanoplastics from liquid medium. By using a portable Raman instrument, our method offers cost-effective, rapid, and field-deployable detection features with excellent sensitivity in nanoplastic analysis with a limit of detection of 0.1 ppm. Moreover, this study provides a highly promising strategy for the robust and sensitive analysis of a wide range of particle analytes through the effective labeling performance of L-MPNs when coupled with SERS techniques.

Environmental Implication

Nanoplastics in ecosystems are emerging "hazardous materials" due to their potential health risks. The novel strategy described in this study, utilizing luminescent metal–phenolic networks (L-MPNs) labeling and surface-enhanced Raman spectroscopy (SERS), enables rapid, sensitive and field-deployable detection of various sizes (50-500 nm) and types of nanoplastics at ultra-low concentrations. Our approach not only aids in the separation of nanoplastics from aquatic mediums but also facilitates rapid quantification of these contaminants, thereby presenting a significant leap towards addressing the critical environmental challenge of nanoplastics contamination.

1. Introduction

The increasing concern surrounding plastic pollution is a global issue, with reports suggesting that by 2050, approximately 12,000 metric tons of plastic waste will either reside in landfills or contaminate the natural environments [1]. Recently, nanoplastics (1–1000 nm) and microplastics (> 1 μm) resulting from the breakdown of larger plastic entities have been identified as significant environmental threats to human health [2,3]. Nanoplastics are more hazardous than microplastics due to their minimized dimensions and the larger specific surface area, which increases their capacity to adsorb toxins [4]. A growing body of research has highlighted the potential health implications linked to nanoplastics, including disturbances in vascular endothelial cadherin connections, initiation of intense inflammatory responses, and alterations in the gut microbiome structure and function [5–7].

Recent advancements in nanoplastics analysis leverage various methods such as Pyrolysis–Gas Chromatography/Mass Spectrometry (Pyrolysis–GC/MS) [8], Attenuated Total Reflectance Fourier-transform Infrared Spectroscopy (ATR-FTIR) [9], and Transmission Electron Microscopy (TEM) [10]. These methodologies, however, require tedious laborious processes, complex instrumentation, and considerable operational expenses. The surface-enhanced Raman scattering (SERS) technique, which intensifies the Raman scattering signals of molecules adsorbed on nanostructured surfaces, stands as a robust analytical tool for highly sensitive quantification [11]. The efficiency of SERS measurements, further augmented by using portable instruments or devices, paves the way for rapid and on-site detection [12,13]. However, the current application of SERS for nanoplastics detection faces challenges. The intrinsic weak signals from various types of nanoplastics due to the intrinsic low scattering cross-section results in low detection limits [14]. While several studies make efforts in development of novel SERS substrates to improve detection performance, this also involves labor-intensive processes, and it still remains challenging to achieve sub ppm detection limits [15]. For example, Chang et al. devised a novel nanowell-enhanced Raman spectroscopy using SiO_2 adorned with silver films (SiO_2 PC@Ag), achieving detection limits of 0.5 ppm for polystyrene (PS) nanoplastics [16]. The substrate synthesis may also involve complex steps, resulting in a total processing time of more than 12 hours [16].

Metal phenolic networks (MPNs), a distinct class of metal-organic compounds derived from metal ions and phenolic entities, showcase remarkable adhesion to an extensive range of surfaces, attributable to the innate attributes of polyphenols. These networks can rapidly (~5 min) adhere to a broad types of particle surfaces (e.g., organic, inorganic, biological) [17–19] and exhibit colloidal stability across diverse aqueous conditions (e.g., high-salt, acidic, alkaline) [20,21]. Moreover,

MPNs can interact with various dyes to form luminescent MPNs (L-MPNs) with a rapid and simple process. L-MPNs have exhibited exceptional efficacy in particle labeling by producing ultrathin luminescent coatings, retaining their fluorescence stability across varied environments (e.g., distinct pH levels, serum, cellular cytosol) [22]. Our prior research demonstrated the utilization of L-MPNs consisting of zirconium ions (Zr^{4+}), tannic acid, and rhodamine B for micro-and nanoplastic labeling, facilitating successful concentration and imaging of plastic particles using a portable microscope [23]. A SERS tag is generated by binding intrinsically strong Raman scattering molecules, known as Raman reporters, onto the surface of plasmon-resonant gold or silver nanoparticles and this process results in a unique SERS spectrum for the Raman reporter, facilitating the sensitive detection of target analytes with weak Raman signals. Importantly, the dyes in L-MPNs labeled nanoplastics have the potential to function as Raman reporters, substantially enhancing the weak signals of nanoplastics through direct SERS measurements.

Herein, we employed tannic acid (TA), Zr^{4+}, and rhodamine B to generate L-MPNs for labeling diverse types of nanoplastics, including 50 nm and 500 nm PS, 500 nm Polymethyl Methacrylate (PMMA), and 250 nm Polylactic acid (PLA). The uniform coating layer of L-MPNs onto nanoplastics was confirmed by dynamic light scattering (DLS), zeta potential, and Confocal Laser Scanning Microscopy (CLSM) measurements. By using 50 nm gold nanoparticles as the SERS substrate and a portable Raman instrument, we investigated the performance of L-MPNs-to facilitate effective separation of nanoplastics and their function as SERS tags for the rapid, sensitive and on-site detection of various concentrations of nanoplastics (AuNPs). Three regression models were compared to establish the correlation between Raman reporter RhB signals and nanoplastic concentrations, ensuring precise quantitative assessments. We also demonstrated the capability of our approaches for the detection of nanoplastics in real-world environmental samples. To the best of our knowledge, this is the first study to apply L-MPNs labeling coupled with SERS for the simple, rapid and sensitive detection of particle analytes. Our research provides great potential in the detection of a wide range of particle analytes (e.g., microplastics, engineered nanomaterials, microorganisms. etc) using L-MPNs labeling-enabled SERS approaches.

2. Methods

2.1. Chemical and materials

Polystyrene (PS) particles with sizes of 500 nm and 50 nm, as well as polymethyl methacrylate (PMMA) particles of 500 nm, were purchased from Phosphorex (Hopkinton, MA, USA). Polylactide (PLA) particles with a size of 250 nm were purchased from CD Bioparticles

(Shirley, NY, USA). Tannic acid (≥99%, ACS reagent) and zirconyl chloride octahydrate ($ZrOCl_2 \cdot 8H_2O$, 98%) were obtained from VWR (Alberta, Canada). Gold nanoparticles (AuNPs, 50 nm ± 4 nm at a concentration of 1 mg/L) were purchased from nanoComposix (San Diego, CA, USA). Double-distilled water (DD water) was provided by the Department of Food Nutrition and Health at University of British Columbia (UBC). Tap water samples were collected from the Department of Food Nutrition and Health. Lake water samples were sourced from Nitobe Memorial Garden at UBC campus, while seawater samples were obtained from Wreck Beach at UBC campus.

2.2. Preparation of nanoplastics labeled by L-MPNs

Nanoplastic solutions (comprising 500 nm PS, 50 nm PS, 500 nm PMMA, and 250 nm PLA) were adjusted to concentrations ranging from 0 to 100 ppm. The L-MPNs@NPs were prepared by combining 20 μL of TA (0.5 mM), 20 μL of $ZrOCl_2 \cdot 8H_2O$ (20 mM), and 20 μL of RhB (0.5 mM) with 940 μL of nanoplastic aqueous suspension, yielding final concentrations of 10 μM TA, 400 μM Zr^{4+}, and 10 μM RhB. After vortexing for 1 min, the mixture was centrifuged at 7500 rpm for 10 min using a mini centrifuge. The supernatant was removed, and the sediments were resuspended in 1 μL of deionized water, producing the desired nanoplastics labeled by L-MPNs (L-MPNs@NPs). .

2.3. SERS measurements of nanoplastics labeled by L-MPNs

The AuNPs solution was employed as the SERS substrate and diluted in a concentration of 0.5 mg/mL using DD water. 1 μL of AuNPs solution was dropped onto aluminum foil, followed by an equivalent volume of L-MPNs@NPs samples. After drying under room temperature conditions for 10 min, the representative Raman spectra at the coffee ring edge were acquired using a WP 785 ER Raman Spectrometer, with a 785-nm laser. Spectra acquisitions were obtained using 450 mW power, 60 s integration, and a spectral range of 300–2008 cm^{-1}. Data processing entailed boxcar smoothing and polynomial baseline adjustments.

2.4. Characterization of L-MPNs labeling

To evaluate the effect of L-MPNs labeling on nanoplastics, we conducted a series of experimental measurements including Dynamic light scattering (DSC), zeta potential, fluorescence and Confocal laser scanning microscopy (CLSM) measurements. All measurements were performed after the removal of the supernatant from nanoplastic samples, followed by the addition of 1 mL of distilled water, except for CLSM and DIC analyses where 100 μL was utilized. DLS and zeta potential assessments were obtained using a Litesizer 500 (Anton Paar, Graz, Austria)

for pure nanoplastics, nanoplastics labeled by MPNs (MPNs@NPs) and L-MPNs@NPs samples. Fluorescence spectroscopy measurements were conducted on a Tecan infinite 200Pro plate reader (excitation at 550 nm; emission at 595 nm) for pure nanoplastics, nanoplastics labeled by RhB (RhB@NPs) and L-MPNs@NPs samples. CLSM for L-MPNs@NPs was performed with a Leica TCS SP5 laser scanning confocal microscope (Wetzlar, Germany) using an HCX PL APO 100x/1.4 OIL objective, 561 nm laser, PMT detectors, and operated with Leica Application Suite AF software.

2.5. Quantitative analysis of nanoplastics by regression model fitting

Raman peak intensity at 1357 cm^{-1} (from RhB) versus nanoplastic concentrations was modeled using three regression equations: Logistic (1), Polynomial (2), and Linear (3). Concentrations above Limit of Detection (LOD) were considered, ranging from 0.1-50 ppm for 500 nm PS and 1-100 ppm for 50 nm PS, 500 nm PMMA and 250 nm PLA. The R^2 value was used to assess model fitting, with model linearization executed by adjusting the concentration axis.

$$f(x) = \frac{a}{1 + e^{-c(x-b)}} \tag{1}$$

$$f(x) = ax^2 + bx + c \tag{2}$$

$$f(x) = ax + b \tag{3}$$

2.6. Nanoplastics detection in real-world scenarios

To simulate nanoplastics in real-world scenarios, we spiked various nanoplastics (500 nm PS, 50 nm PS, 500 nm PMMA, and 250 nm PLA) at concentration of 10 ppm into tap, lake and sea water, respectively. The same procedure as in section 2.2 was then employed for these nanoplastics samples to prepare L-MPNs@NPs. The concentration of spiked nanoplastics was determined through corresponding established regression curves. The recovery ratio was calculated as the following equation:

$$\text{Recovery ratio} = \frac{C_1}{C_2} \times 100\% \tag{4}$$

Where C_1 is the determined nanoplastics concentration and C_2 is the spiked nanoplastics concentration (10 ppm).

2.7. Statistical analysis.

Experiments were replicated thrice, and results are presented as mean ± SD. Data underwent one-way ANOVA analysis using SPSS 18.0 (IBM Corp., Armonk, NY, USA), considering a significance threshold of $p < 0.05$.

3. Results and discussion

3.1. Formation and Separation of L-MPNs@NPs

L-MPNs labeling of nanoplastics can cause the surface modification of plastic particles with L-MPNs through a simple self-assembly process (Figure 1a) [22]. We hypothesized that nanoplastics can be uniformly labeled by the L-MPNs and that these labeling strategies can further facilitate the efficient separation of L-MPNs@NPs by centrifugation. To demonstrate the efficacy of L-MPNs labeling onto nanoplastics, a synergistic approach utilizing both spectroscopic and microscopic techniques was employed. As an example, PS nanoplastics with a particle size of 500 nm were employed. Results presented in Figure 1b reveal a decline in the zeta potential following the formation of MPNs labeled nanoplastics (MPNs@NPs) (-16.41 ± 1.16 mV) compared to pure NPs (-9.27 ± 1.23 mV). This indicates the successful labeling of MPNs onto the surface of NPs due to the deprotonation of TA [22]. Moreover, the subsequent incorporation of RhB into MPNs coating accentuated the zeta potential to -8.74 ± 0.37 mV due to the high zeta potential of RhB (-0.86 ± 0.50 mV) in the experimental setting, indicating a successful L-MPNs labeling of nanoplastics. This L-MPNs labeling was further investigated by CLSM and DIC microscopy, and the images showed the RhB signals localized on the surface of the NPs (Figure 1c–d). In addition, to further demonstrate the effect of L-MPNs on fluorescence labeling of nanoplastics, we used fluorescence spectroscopy to compare the fluorescence intensities of NPs mixing with RhB alone and L-MPNs@NPs. A substantial amplification in fluorescence intensity was observed with L-MPNs@NPs (28514 ± 295) compared to NPs alone subjected to RhB (1773 ± 52), illustrating the important role of MPNs coating in enhancing the efficacy of RhB binding (Figure 1e).

The precipitation of NPs is crucial for their separation, but conventional centrifugation techniques prove to be ineffective in facilitating precipitation, primarily due to the low molecular weight of NPs. Previous research indicates that continuous flow centrifugation operated at 10,000 rpm can effectuate the direct separation of 160 nm nanoplastics [24]. However, it requires bulky centrifugation apparatus and extended processing times (> 7 h). In contrast, the L-MPNs labeling strategy offers a promising avenue for NPs separation by employing portable mini-centrifugation devices quickly (in 10 min) [23]. The enlargement in particle size was observed for both MPNs@NPs (782 ± 138 nm) and L-MPNs@NPs (912 ± 94 nm) post-centrifugation compared to

198 pure NPs (420 ± 9 nm), implying a potential role of L-MPNs in promoting NPs separation through
199 aggregation (Figure 1f). This effect is markedly pronounced for smaller NPs (50 nm), with
200 significant size increase post synthesis of MPNs@NPs and L-MPNs@NPs from 48 ± 1 nm to 1365
201 ± 385 nm and 1180 ± 494 nm, respectively, as documented in Figure S1. Furthermore, both CLSM
202 and DIC imaging revealed that 50 nm NP aggregates were induced by L-MPNs labeling (Figure
203 S2). Therefore, we demonstrate that L-MPNs exhibit dual functionality: Forming uniform coatings
204 on the surface of NPs and facilitating a more streamlined separation process of NPs through the
205 utilization of portable centrifugation machines.

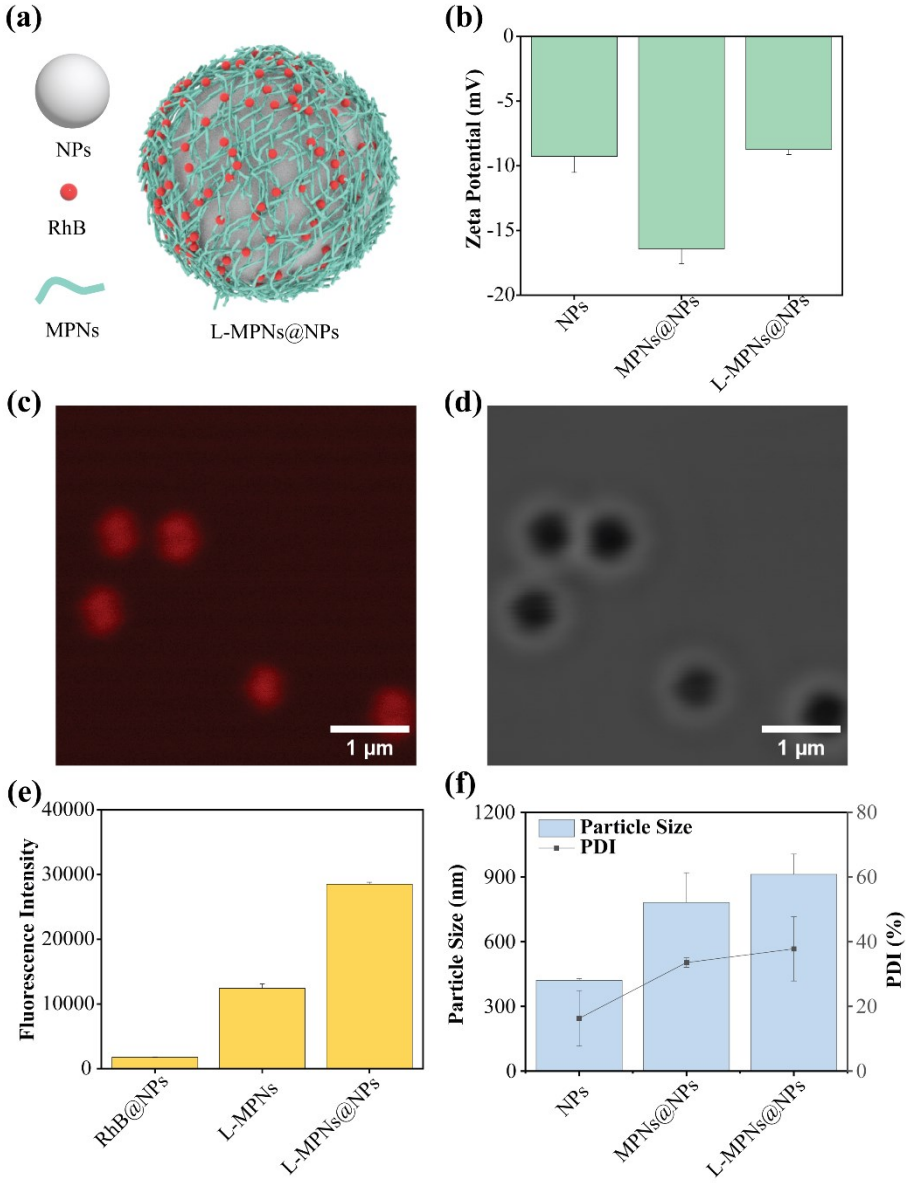

206

207 **Figure 1. Characterization of nanoplastics labeled by L-MPNs.** (a) Illustration of the self-

assembly process forming L-MPNs@MNPs. (b) Zeta potential changes following the formation of MPNs@NPs and L-MPNs@NPs. CLSM (c) and DIC (d) images of L-MPNs@NPs, respectively. (e) Fluorescence intensity measurements of NPs labeled with RhB and L-MPNs as well as L-MPNs in the absence of NPs. (f) Particle size changes following the formation of MPNs@NPs and L-MPNs@NPs, in comparison to pure NPs. Data are presented as mean ± SD in bar charts.

3.2. Optimization of SERS analysis

The SERS technique is a powerful analytical tool renowned for its high sensitivity. This method amplifies the Raman scattering signals of molecules adsorbed onto nanostructured metal substrates, thereby facilitating the sensitive and quantitative analysis of molecules, even at ultralow concentrations [25]. In this study, AuNPs were chosen as the SERS substrate. We hypothesized that L-MPNs could not only facilitate the separation of nanoplastics, but also serve as a robust Raman reporter for nanoplastics detection by substituting the intrinsic signals from nanoplastics (Figure 2a). Raman reporters are Raman-intensive molecules that have a strong affinity for the metal surface [26]. Dyes such as RhB are commonly used as Raman reporters, but direct labeling of these dyes for nanoplastics is not ideal due to limited binding. However, incorporating RhB with MPNs to form the L-MPNs may facilitate the efficient Raman labeling of nanoplastics. By using this approach, the intrinsic peak intensity (433 ± 114) from PS NPs at 998 cm^{-1} was substituted by the heightened value (18043 ± 1895) originating from RhB in L-MPNs at 1357 cm^{-1} (Figure 2b), indicating a promising avenue to improve the sensitivity of SERS approaches for PS detection.

To demonstrate the performance of utilizing Rhodamine B as a Raman reporter in L-MPNs-based SERS tags, components of L-MPNs@NPs were characterized using SERS measurements (Figure 2c). Notably, AuNPs showed negligible signals spanning the entire spectrum and 500 nm PS NPs exhibited a characteristic peak at 998 cm^{-1}, attributed to ring-breathing modes. Furthermore, RhB displayed several characteristic peaks, with the peak at 1357 cm^{-1} showcasing the utmost intensity and this peak was also observed in TA. The peaks at 1357 cm^{-1} for RhB and TA are attributed to aromatic C-C stretching vibrations [27] and C-O vibration [28], respectively. Following the labeling of NPs with MPNs, 500 nm PS NPs maintained their characteristic peaks. However, upon the incorporation of RhB, the signals were covered by RhB due to the substantial Raman activity of RhB.

The optimization of the AuNPs substrate concentration was conducted by monitoring the Raman intensity of the characteristic peaks at 998 cm^{-1} originating from pure PS NPs (Figure 2d–e). It was observed that increasing the concentration of AuNPs from 0.01 to 0.5 mg/L resulted in an augmented peak intensity from 75 ± 9 to 2162 ± 79 at 998 cm^{-1}, a phenomenon attributed to the

increased SERS enhancement area provided by the AuNPs. However, further concentration increase (from 0.5 to 1 mg/L) led to a decline in peak intensity (down to 1777 ± 68). Consequently, an AuNPs concentration of 0.5 mg/L was selected, owing to its exhibition of the highest peak intensity. Furthermore, RhB concentration was optimized, with the characteristic peak at 1357 cm^{-1} used for subsequent analyses (Figure 2f–g). An ascending trend in peak intensity (from 787 ± 27 to 9285 ± 417) was observed as RhB concentration varied from 2 to 10 μM, and a decrease (down to 4892 ± 27) was observed with further concentration increments (10 to 20 μM). Increasing the concentration to 40 μM resulted in signal saturation with the detector, making it unsuitable for SERS analysis. Thus, an optimized RhB concentration of 10 μM was determined for subsequent quantitative investigations.

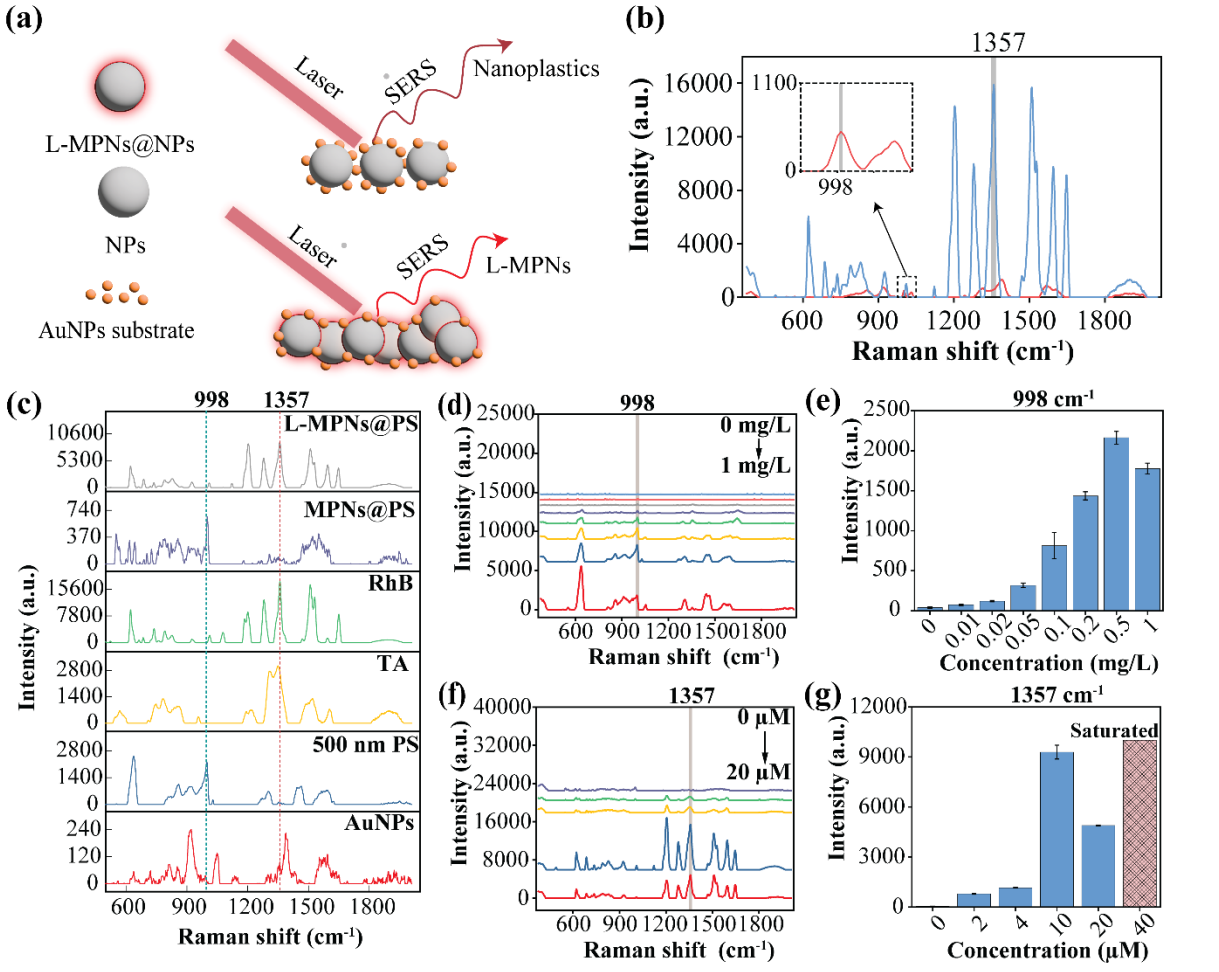

Figure 2. The optimization of AuNPs and RhB concentrations for SERS Analysis. (a) Schematic illustration of the detection of nanoplastics using L-MPNs labeling via SERS techniques. (b) SERS spectra of pure nanoplastics solution and L-MPNs@NPs (500 nm PS with concentration of 50 ppm) following centrifugation. (c) SERS spectra of various components (TA, RhB, PS,

MPNs@NPs, L-MPNs@NPs) derived from L-MPNs@NPs in the presence of AuNPs. (d) SERS spectra of 10 ppm PS NPs in conjunction with AuNPs solutions at varying concentrations: 0, 0.01, 0.02, 0.05, 0.1, 0.2, 0.5, and 1 mg/L. (e) Variation in the characteristic peak intensity of PS at 998 cm^{-1} with AuNPs concentrations ranging between 0 and 1 mg/L. (f) SERS spectra of L-MPNs@NPs (sourced from 10 ppm PS NPs) with diverse RhB concentrations: 0, 2, 4, 10, 20, and 40 μM. (g) Raman intensity in the characteristic peak of RhB at 1357 cm^{-1} corresponding to RhB concentrations spanning from 0 to 40 μM. Data are presented as mean ± SD in bar charts.

3.3. SERS detection of various sizes and types of NPs

Nanoplastics in environmental systems may exist in various sizes and types, which enhances the difficulty of their identification. To demonstrate the applicability of L-MPNs labeling-enabled SERS approaches for the detection of a wide range of nanoplastics, we used this SERS method for the analysis of diverse sizes and types of nanoplastics. We first investigated the SERS spectra of L-MPNs@PS NPs with 50 nm and 500 nm sizes over a concentration gradient from 0 to 100 ppm to explore the size factor (Figure 3a&3c). Both spectra of 50 nm and 500 nm PS NPs after L-MPNs labeling displayed a consistent fingerprinting pattern of RhB. The characteristic peak of RhB at 1357 cm^{-1} was positively correlated with the concentration of nanoplastics and was used for the quantification studies (Figure 3b&3d). The LOD of the assay was determined. For the 500 nm PS NPs, RhB characteristic peak intensity remains negligible changes between concentrations of 0 and 0.05 ppm but increases from 0.1 to 50 ppm. The LOD of SERS detection of 500 PS NPs is determined as 0.1 ppm via one-way ANOVA analysis, signifying statistically significant difference ($p < 0.05$) comparing to lower concentrations. Increasing the concentration further from 50 ppm to 100 ppm for 500 nm PS NPs caused the RhB signal decreased, possibly due to an inhibition of the resonance Raman effect caused by aggregation [29]. 50 nm PS NPs exhibited a similar RhB signal change over concentrations (Figure 3d). The LOD for the detection of 50 nm PS NPs was determined at 1 ppm. Notably, the decrease in RhB peak intensity when analyzing 50 nm PS particles was observed in comparison to 500 nm PS particles over the same concentration beyond the LOD. This could be attributed to the enhanced nanoplastics aggregation mediated by L-MPNs (Figure S2) for 50 nm PS NPs which might reduce the resonance Raman effect [29].

The efficacy of the L-MPNs labeling strategy was further evaluated for the detection of other types of nanoplastics, including PMMA and PLA (Figures 3e&3g). LOD for the analysis of both 500 nm PMMA and 250 nm PLA nanoplastics was determined as 1 ppm after one-way ANOVA analysis ($p < 0.05$) (Figure 3f&3h). It can be seen that quantification proficiency of the L-MPNs strategy for nanoplastics is type-dependent. The difference of LOD for various types of nanoplastic particles may be attributed to the variation of L-MPNs interaction with particles. For instance, for

the same particle size of 500 nm, PMMA NPs exhibited a slightly different RhB signals pattern compared to the PS NPs. Given the inherent surface property variations across different types of nanoplastics, their respective interactions (e.g., electrostatic interactions, hydrogen bonding, and van der Waals forces) with L-MPNs vary, resulting in differential RhB binding efficacies [30,31]. The enhanced RhB signals was observed for 500 nm PS NPs compared to 500 nm PMMA, potentially attributed to π-π interactions caused by the benzenol units in PS NPs and the L-MPNs coating [22], which facilitate the adhesion of L-MPNs onto the surface of PS NPs. The same phenomenon was observed for 250 nm PLA as compared to 500 nm PS NPs. This conclusively indicates that L-MPNs labeling-enabled SERS approaches show excellent performance in the detection of a wide range of sizes and types of nanoplastics.

Comparably, we also evaluated the LOD of the SERS assay for the detection of nanoplastics without L-MPNs-mediated labeling and separation (Figure S3a–h). For PS, PMMA, and PLA, the characteristic Raman peaks were identified at 1002 cm^{-1}, 811 cm^{-1}, and 870 cm^{-1}, respectively [32–34]. The LOD was determined at 50 ppm for both 500 nm PS and PMMA, and 100 ppm for 50 nm PS. No characteristic peak was found for 250 nm PLA at a concentration of 100 ppm (Figure S3g–h). The comparison of LOD of different SERS assays is displayed in Table 1. These results showed that L-MPNs-mediated labeling and separation approach can greatly enhance the sensitivity of nanoplastics detection.

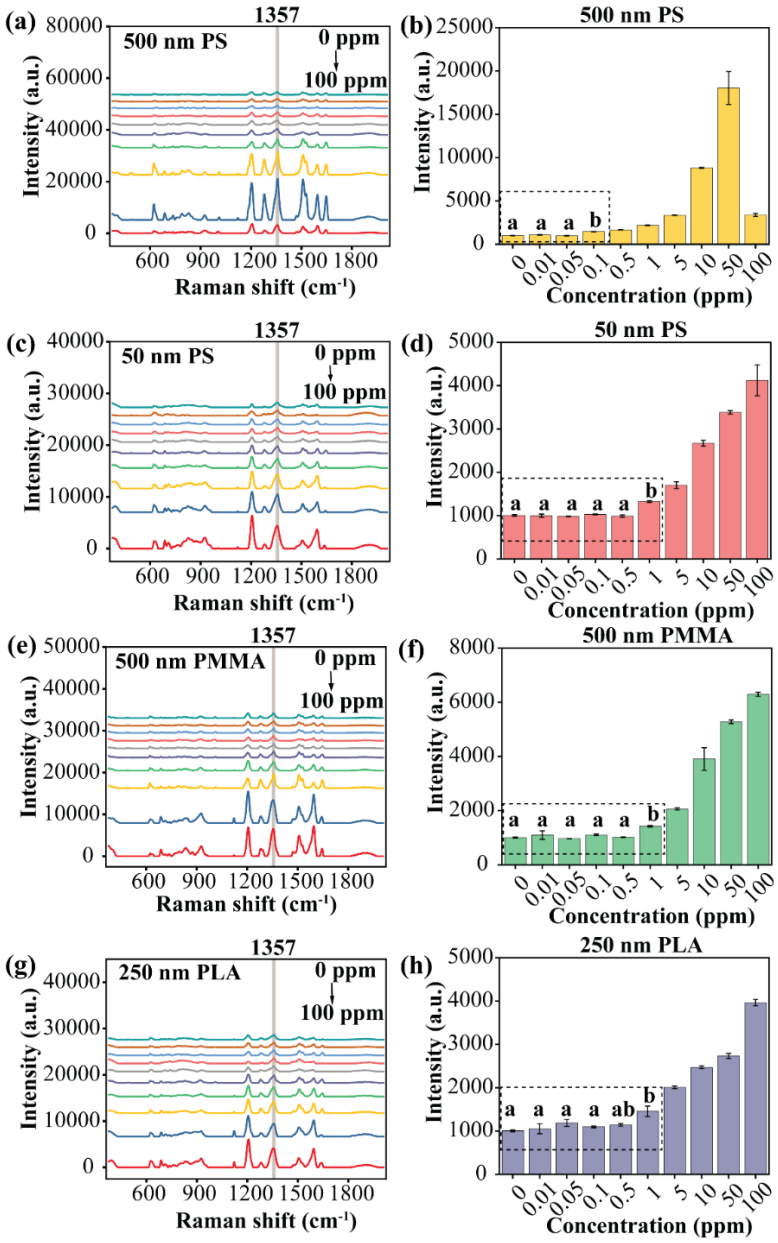

308

309 **Figure 3.** SERS detection of nanoplastics with diverse types and sizes utilizing L-MPNs mediated
310 labeling and separation. SERS spectra of L-MPNs@NPs at different concentrations (0, 0.01, 0.05,
311 0.1, 0.5, 1, 5, 10, 50, 100 ppm): (a) 500 nm PS, (c) 50 nm PS, (e) 500 nm PMMA, and (g) 250 nm
312 PLA. Depiction of the correlation between the RhB characteristic peak intensity at 1357 cm^{-1} and
313 nanoplastic concentrations for the following nanoplastics: (b) 500 nm PS, (d) 50 nm PS, (f) 500
314 nm PMMA, and (h) 250 nm PLA. Data are represented as mean ± SD in bar charts. Distinct letter
315 notations (a, b) within the figure highlight significant differences ($p < 0.05$), as determined by one-
316 way ANOVA.

Table 1. Comparison of LOD of SERS analysis of NPs with and without L-MPNs labeling

Types	Sizes	LOD (with L-MPNs)	LOD (without L-MPNs)
PS	500 nm	0.1 ppm	50 ppm
PS	50 nm	1 ppm	100 ppm
PMMA	500 nm	1 ppm	50 ppm
PLA	250 nm	1 ppm	>100 ppm

3.4. Quantification analysis of nanoplastics

Following the demonstration of the high performance of SERS analysis of nanoplastics using RhB as a Raman reporter, we further performed quantitative analysis of nanoplastics using this method. In a SERS spectrum, these peak intensities exhibit a proportional relationship to the analyte concentration, thus facilitating accurate and high-precision quantitative analysis [35,36]. We evaluated three regression models, including logistic, polynomial, and linear, to display the relationship between nanoplastic concentrations and RhB signals. Concentration gradients exceeding the LOD, elaborated in Section 2.3, served as sample groups for the quantification analysis.

As shown in Figure 4a–c, when examining 500 nm PS nanoplastics, the polynomial model (R^2 = 0.9867) outperforms both its logistic (R^2 = 0) and linear (R^2 = 0.9398) counterparts in predictive proficiency, thus polynomial regression is selected as the optimal model. Polynomial regression consistently excelled in performance when diverse nanoplastic sizes and types were analyzed (Figure S4). To streamline data interpretation, we adjusted the fitting curves for all nanoplastic samples by recalibrating the X-axis to make the curves linear. The adjusted plots were displayed in Figures 4d–g, representing 500 nm PS, 50 nm PS, 500 nm PMMA, and 250 nm PLA respectively. It is imperative to underscore that the quantitative relationship varies based on both size and type. This underscores the importance to determine nanoplastics' size and type through characterization methodologies before ensuring accurate quantification. Consequently, these findings further emphasize the effectiveness of our L-MPNs-mediated labeling and separation coupled with SERS assay in quantifying various types and sizes of nanoplastics.

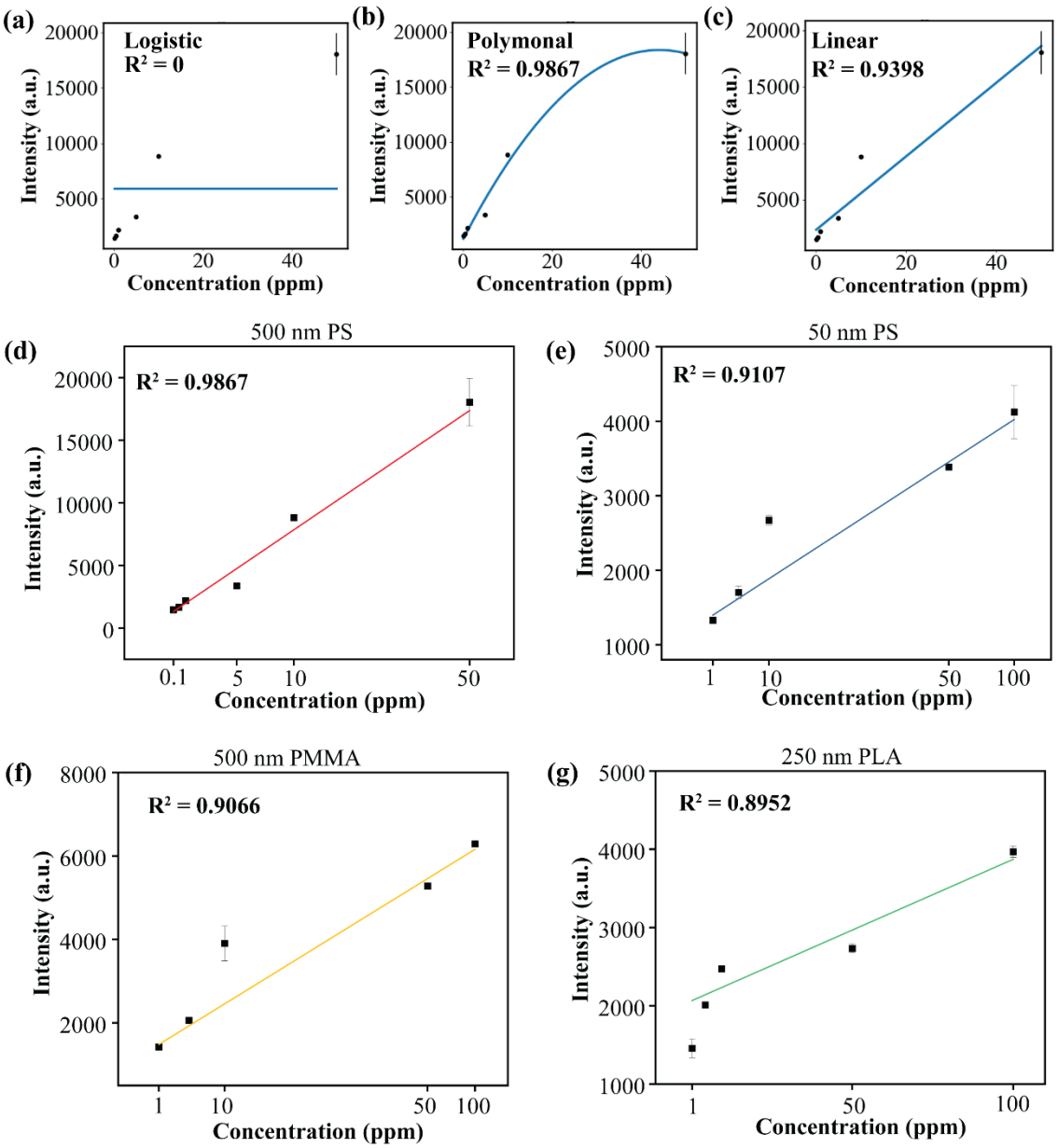

Figure 5. Quantitative analysis of L-MPNs@NPs using regression models. Investigation of the relationship between 500 nm PS nanoplastic concentration and the SERS characteristic peak intensity at 1357 cm^{-1} from RhB employing distinct regression models: (a) logistic, (b) polynomial, and (c) linear. Linearized curves resulting from X-axis recalibration of the polynomial regression curves for different sizes and types of nanoplastics: (d) 500 nm PS, (e) 50 nm PS, (f) 500 nm PMMA, and (g) 250 nm PLA. Data are denoted as mean ± SD.

3.5. Detection of nanoplastics in real-world environmental samples

Nanoplastics have been identified in various environmental settings, particularly water

systems, and the detection of nanoplastics in real environmental water remains a challenge [37]. To demonstrate the efficacy of our SERS method for the detection of nanoplastics in real-world scenarios, we introduced nanoplastics (10 ppm) with varying sizes and types (500 nm PS, 50 nm PS, 500 nm PMMA, and 250 nm PLA) into tap, lake, and seawater samples. Subsequently, we use the developed SERS method to detect and quantify these nanoplastics.

To evaluate any potential interference substances coming from the water systems, SERS spectra of water systems were first obtained after direct addition of L-MPNs into water systems without addition of nanoplastics (Figure S5a). It is evident that both lake water and tap water systems displayed a SERS fingerprinting spectrum analogous to that of DD water. In contrast, spectra from seawater reveal two additional peaks at 790 and 829 cm^{-1}. Notably, for the RhB characteristic peak at 1357 cm^{-1} employed in quantitative analysis, the peak intensity from tap water showed no significant deviation ($p > 0.05$) compared to DD water while lake and sea water indicated a significant difference ($p < 0.05$) (Figure S5b). The primary constituents of tap water include minor soluble minerals (e.g., Ca^{2+}, Mg^{2+}, K^{+}, and Cl^{-}), that lead to the interference in the detection. Beyond these minerals, lake water may contain biological entities, including bacteria, protozoans, and algae [38]. These biological entities can be labeled by MPNs [39], contribute to an increase in the SERS signals. This effect is even more pronounced in seawater, which may contain larger amounts of microbial load and minerals [40]. These results indicate that the real-world environmental water contains substances that could interfere with the SERS assay.

To achieve accurate detection of nanoplastics by eliminating potential interference from the water systems and in real-world settings, our SERS signals from nanoplastics were established by subtraction of SERS signal intensity of RhB in at 1357 cm^{-1} by the corresponding control signals (signals from environmental water without nanoplastic addition). After spiking of different sizes and types of nanoplastics (10 ppm) in these environmental water systems, SERS measurements for nanoplastics, after L-MPNs mediated separation and labeling, showed similar spectral patterns (Figure 6a–d) as RhB. This demonstrates that RhB as a Raman reporter can be successfully labeled onto nanoplastics. We further evaluated the recovery ratios of nanoplastics of varied types and sizes at a concentration of 10 ppm when spiked into these water systems. All acquired SERS peak intensities at 1357 cm^{-1} had subtracted the corresponding control signals (environmental water without nanoplastic addition) to obtain the real nanoplastics signals. The recovery ratios were calculated by dividing the real signals from nanoplastics in various water systems by those in DD water systems. As illustrated in Figure 6e, all nanoplastic samples in tap and lake water yielded good recovery ratios (90 – 120%). The recovery ratio for nanoplastics in seawater was below 60%. This may arise from several factors. For example, the larger amounts of biological entities and

salts may interact with nanoplastics and affect the L-MPNs labeling. The salts in the sea water may lead to AuNPs aggregate and affect the SERS substrate performance[41]. Altogether, these results showed that L-MPN labeling-enabled SERS methods can quantitatively analyze nanoplastics in real-world environmental setting.

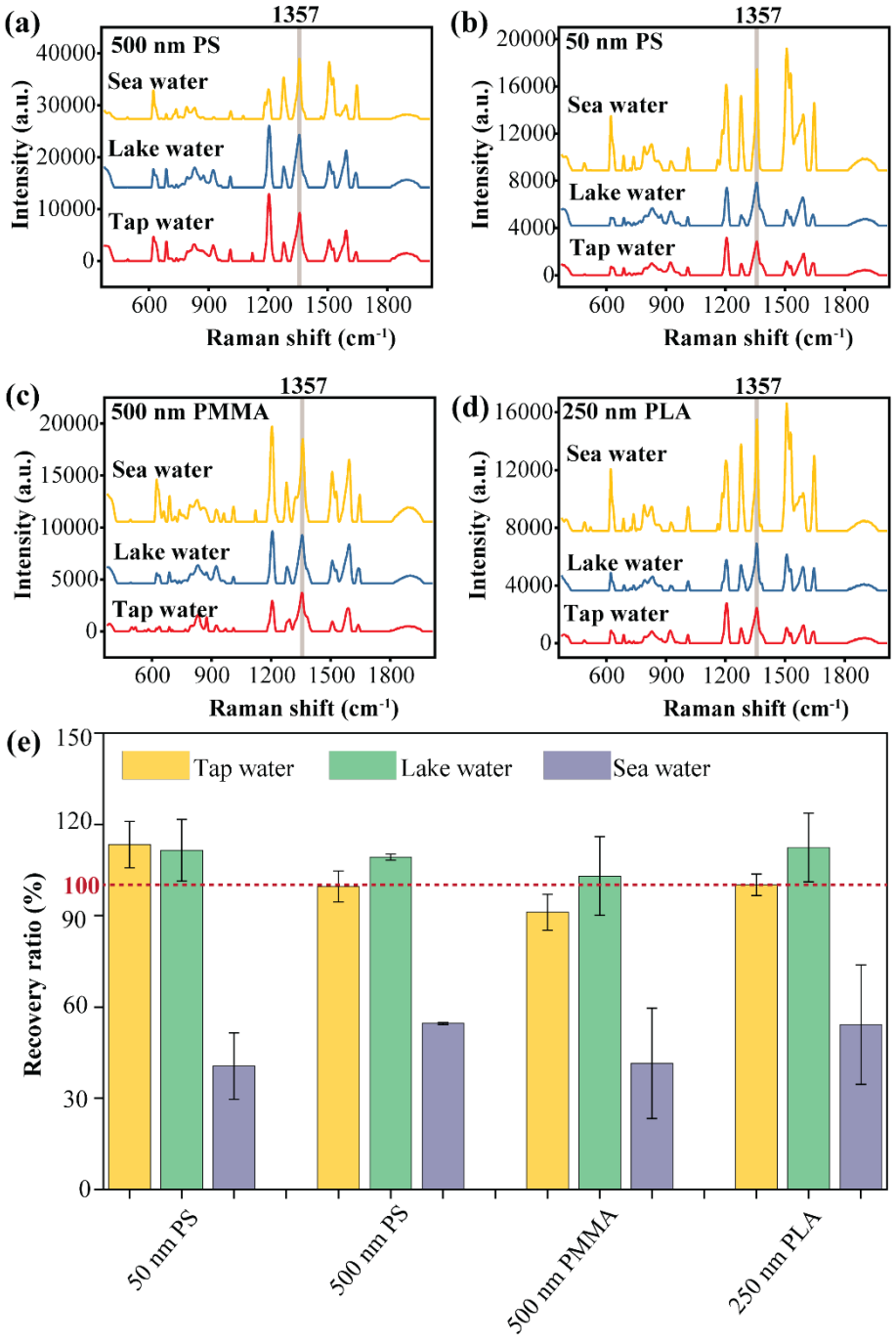

Figure 6. Quantitative analysis of nanoplastics in diverse environmental samples. The SERS spectra of 500 nm PS (a), 50 nm PS (b), 500 nm PMMA (c), and 250 nm PLA (d) nanoplastics

introduced into various water sources (tap, lake, and sea) at a concentration of 10 ppm using L-MPNs-mediated methods. (e) Recovery ratios for various nanoplastics (500 nm PS, 50 nm PS, 500 nm PMMA, 250 nm PLA) at a concentration of 10 ppm spiked in tap, lake, and seawater. Data are presented as mean ± SD. The different letters (a–c) within the figure indicate significant differences ($p < 0.05$).

3.6. Comprehensive analysis of our SERS method

To highlight the strength of our method, we compared it with recent Raman techniques for nanoplastic detection. This comparison focused on three key factors: LOD, cost, and the operation time. Previously, much of the research has been directed towards enhancing the LOD by utilizing advanced surface-enhanced Raman scattering (SERS) substrates [42–44]. Nonetheless, two main obstacles arise: some materials involve complex synthesis, while others face relatively high commercial costs. Additionally, many researchers conducted pre-treatments such as vacuuming, filtration or drying to facilitate nanoplastic concentration [45,46]. These steps, however, could add several hours to the overall procedure [47]. Contrastingly, our innovative SERS tag approach integrating L-MPN labeling and AuNPs as SERS substrates offers time-efficient, cost-friendly, and high-sensitivity features, which stands out when compared to much of the existing work [15,46]. By using only small amounts of the AuNPs solution and sample (1 μL each), our approach also showed practical large-scale detection capabilities. Our L-MPNs-based separation process not only cuts down the detection time to around 30 minutes but also offers an impressive LOD of 0.1 ppm for 500 nm PS and 1 ppm for other varieties such as 50 nm PS, 500 nm PMMA, and 250 nm PLA, achieving a maximal of 500-fold sensitivity improvement in comparison to direct detection methods. With the use of a portable Raman device and a mini centrifuge, our method is well suited for rapid and on-site testing. The broad labeling approach using L-MPNs further suggests that our method could be expanded for testing other analytes, potentially ensuring long-term safety in environmental and agri-food systems.

Conclusion

This study introduces a pioneering approach leveraging L-MPNs for the rapid and effective separation and labeling of nanoplastics. The innovative strategy of employing RhB as a Raman reporter has demonstrated a significant pathway to achieve great sensitivity improvements in the detection of nanoplastics with diverse sizes and types, including 0.1 ppm for 500 nm PS and 1 ppm for 50 nm PS, 500 nm PMMA, and 250 nm PLA. Polynomial regression performed as the most proficient model for accurate nanoplastic quantification across diverse sizes and types among the tested regression models. The high recovery ratios were observed for nanoplastics detected in real environmental water systems, including tap and lake water. In comparison to other SERS techniques for nanoplastic detection, our method demonstrated superior performance such as lower LOD, cost-effective measurements, and time-efficient operation. The versatility of the L-MPNs labeling strategy provides a promising solution for rapid and sensitive detection of a wider array of nanoplastic variants and other particulate matters, and thereby can significantly contribute to the plastic detection and management strategies in environmental ecosystems.

CRediT authorship contribution statement

Haoxin Ye: Conceptualization, Investigation, Methodology, Writing – original draft.

Guang Gao: Investigation, Methodology.

Tianxi Yang: Conceptualization, Supervision, Funding acquisition, Writing – review & editing.

Declaration of Competing Interest

The authors declare no competing financial interest.

Acknowledgements

This work was supported by the UBC Faculty of Land and Food Systems/Start Up Funds (AWD-020249 UBCLANDF 2022), Natural Sciences and Engineering Research Council of Canada (NSERC) Discovery Grant (RGPIN-2023-04100) and NSERC Discovery Launch Supplement (DGECR-2023-00386). Imaging was performed in the LSI Imaging Core Facility of the Life Sciences Institute at the University of British Columbia, supported by Life Sciences Institute, the UBC GREx Biological Resilience Initiative. The infrastructure within LSI Imaging Core Facility is funded by the Canadian Foundation of Innovation, BC Knowledge Development Fund, Natural Sciences and Engineering Research Council Research Tools and Instruments, and UBC Research Facility Support Grants as well as a Strategic Investment Fund (Faculty of

446 Medicine, UBC).

447 **Appendix A. Supporting information**

448 Supplementary data associated with this article can be found in the online version

449

References

[1] R. Geyer, J.R. Jambeck, K.L. Law, Production, use, and fate of all plastics ever made, Science Advances. 3 (2017) e1700782. https://doi.org/10.1126/sciadv.1700782.

[2] P.M. Gopinath, V.D. Parvathi, N. Yoghalakshmi, S.M. Kumar, P.A. Athulya, A. Mukherjee, N. Chandrasekaran, Plastic particles in medicine: A systematic review of exposure and effects to human health, Chemosphere. 303 (2022) 135227. https://doi.org/10.1016/j.chemosphere.2022.135227.

[3] A.D. Vethaak, J. Legler, Microplastics and human health, Science. 371 (2021) 672–674. https://doi.org/10.1126/science.abe5041.

[4] N. Tang, X. Li, X. Gao, X. Liu, W. Xing, The adsorption of arsenic on micro- and nano-plastics intensifies the toxic effect on submerged macrophytes, Environmental Pollution. 311 (2022) 119896. https://doi.org/10.1016/j.envpol.2022.119896.

[5] W. Wei, Y. Li, M. Lee, N. Andrikopoulos, S. Lin, C. Chen, D.T. Leong, F. Ding, Y. Song, P.C. Ke, Anionic nanoplastic exposure induces endothelial leakiness, Nat Commun. 13 (2022) 4757. https://doi.org/10.1038/s41467-022-32532-5.

[6] M. Teles, J.C. Balasch, M. Oliveira, J. Sardans, J. Peñuelas, Insights into nanoplastics effects on human health, Science Bulletin. 65 (2020) 1966–1969. https://doi.org/10.1016/j.scib.2020.08.003.

[7] M. Wang, Q. Li, C. Shi, J. Lv, Y. Xu, J. Yang, S.L. Chua, L. Jia, H. Chen, Q. Liu, C. Huang, Y. Huang, J. Chen, M. Fang, Oligomer nanoparticle release from polylactic acid plastics catalysed by gut enzymes triggers acute inflammation, Nat. Nanotechnol. 18 (2023) 403–411. https://doi.org/10.1038/s41565-023-01329-y.

[8] C. Li, Y. Gao, S. He, H.-Y. Chi, Z.-C. Li, X.-X. Zhou, B. Yan, Quantification of Nanoplastic Uptake in Cucumber Plants by Pyrolysis Gas Chromatography/Mass Spectrometry, Environ. Sci. Technol. Lett. 8 (2021) 633–638. https://doi.org/10.1021/acs.estlett.1c00369.

[9] L.M. Hernandez, E.G. Xu, H.C.E. Larsson, R. Tahara, V.B. Maisuria, N. Tufenkji, Plastic Teabags Release Billions of Microparticles and Nanoparticles into Tea, Environ. Sci. Technol. 53 (2019) 12300–12310. https://doi.org/10.1021/acs.est.9b02540.

[10] H. Cai, E.G. Xu, F. Du, R. Li, J. Liu, H. Shi, Analysis of environmental nanoplastics: Progress and challenges, Chemical Engineering Journal. 410 (2021) 128208. https://doi.org/10.1016/j.cej.2020.128208.

[11] J.F. Li, Y.F. Huang, Y. Ding, Z.L. Yang, S.B. Li, X.S. Zhou, F.R. Fan, W. Zhang, Z.Y. Zhou, D.Y. Wu, B. Ren, Z.L. Wang, Z.Q. Tian, Shell-isolated nanoparticle-enhanced Raman spectroscopy, Nature. 464 (2010) 392–395. https://doi.org/10.1038/nature08907.

[12] X. He, C. Fan, Y. Luo, T. Xu, X. Zhang, Flexible microfluidic nanoplasmonic sensors for refreshable and portable recognition of sweat biochemical fingerprint, Npj Flex Electron. 6 (2022) 1–10. https://doi.org/10.1038/s41528-022-00192-6.

[13] W. Zhu, B.-Y. Wen, L.-J. Jie, X.-D. Tian, Z.-L. Yang, P.M. Radjenovic, S.-Y. Luo, Z.-Q. Tian, J.-F. Li, Rapid and low-cost quantitative detection of creatinine in human urine with a

portable Raman spectrometer, Biosensors and Bioelectronics. 154 (2020) 112067. https://doi.org/10.1016/j.bios.2020.112067.
[14] N.K. Mogha, D. Shin, Nanoplastic detection with surface enhanced Raman spectroscopy: Present and future, TrAC Trends in Analytical Chemistry. 158 (2023) 116885. https://doi.org/10.1016/j.trac.2022.116885.
[15] L. Xie, K. Gong, Y. Liu, L. Zhang, Strategies and Challenges of Identifying Nanoplastics in Environment by Surface-Enhanced Raman Spectroscopy, Environ. Sci. Technol. 57 (2023) 25–43. https://doi.org/10.1021/acs.est.2c07416.
[16] L. Chang, S. Jiang, J. Luo, J. Zhang, X. Liu, C.-Y. Lee, W. Zhang, Nanowell-enhanced Raman spectroscopy enables the visualization and quantification of nanoplastics in the environment, Environ. Sci.: Nano. 9 (2022) 542–553. https://doi.org/10.1039/D1EN00945A.
[17] H. Ejima, J.J. Richardson, F. Caruso, Metal-phenolic networks as a versatile platform to engineer nanomaterials and biointerfaces, Nano Today. 12 (2017) 136–148. https://doi.org/10.1016/j.nantod.2016.12.012.
[18] Y. Li, Y. Miao, L. Yang, Y. Zhao, K. Wu, Z. Lu, Z. Hu, J. Guo, Recent Advances in the Development and Antimicrobial Applications of Metal–Phenolic Networks, Advanced Science. 9 (2022) 2202684. https://doi.org/10.1002/advs.202202684.
[19] J. Guo, Y. Ping, H. Ejima, K. Alt, M. Meissner, J.J. Richardson, Y. Yan, K. Peter, D. von Elverfeldt, C.E. Hagemeyer, F. Caruso, Engineering Multifunctional Capsules through the Assembly of Metal–Phenolic Networks, Angewandte Chemie International Edition. 53 (2014) 5546–5551. https://doi.org/10.1002/anie.201311136.
[20] X. Zhang, Z. Fan, W. Xu, Q. Meng, C. Shen, G. Zhang, C. Gao, Thin film composite nanofiltration membrane with nanocluster structure mediated by graphene oxide/metal-polyphenol nanonetwork scaffold interlayer, Journal of Membrane Science. 669 (2023) 121330. https://doi.org/10.1016/j.memsci.2022.121330.
[21] J. Chen, S. Pan, J. Zhou, R. Seidel, S. Beyer, Z. Lin, J.J. Richardson, F. Caruso, Metal–Phenolic Networks as Tunable Buffering Systems, Chem. Mater. 33 (2021) 2557–2566. https://doi.org/10.1021/acs.chemmater.1c00015.
[22] Z. Lin, J. Zhou, Y. Qu, S. Pan, Y. Han, R.P.M. Lafleur, J. Chen, C. Cortez-Jugo, J.J. Richardson, F. Caruso, Luminescent Metal-Phenolic Networks for Multicolor Particle Labeling, Angewandte Chemie International Edition. 60 (2021) 24968–24975. https://doi.org/10.1002/anie.202108671.
[23] H. Ye, X. Zheng, H. Yang, M. Kowal, T. Seifried, G.P. Singh, K. Aayush, G. Gao, E. Grant, D. Kitts, R. Yada, T. Yang, Rapid Detection of Micro/Nanoplastics Via Integration of Luminescent Metal Phenolic Networks Labeling and Quantitative Fluorescence Imaging in A Portable Device, (2023). https://doi.org/10.26434/chemrxiv-2023-jnbm1.
[24] L. Hildebrandt, D.M. Mitrano, T. Zimmermann, D. Pröfrock, A Nanoplastic Sampling and Enrichment Approach by Continuous Flow Centrifugation, Frontiers in Environmental Science. 8 (2020). https://www.frontiersin.org/articles/10.3389/fenvs.2020.00089 (accessed September 18, 2023).
[25] B. Sharma, R.R. Frontiera, A.-I. Henry, E. Ringe, R.P. Van Duyne, SERS: Materials,

applications, and the future, Materials Today. 15 (2012) 16–25. https://doi.org/10.1016/S1369-7021(12)70017-2.
[26] C. Zong, M. Xu, L.-J. Xu, T. Wei, X. Ma, X.-S. Zheng, R. Hu, B. Ren, Surface-Enhanced Raman Spectroscopy for Bioanalysis: Reliability and Challenges, Chem. Rev. 118 (2018) 4946–4980. https://doi.org/10.1021/acs.chemrev.7b00668.
[27] S. Huh, J. Park, Y.S. Kim, K.S. Kim, B.H. Hong, J.-M. Nam, UV/Ozone-Oxidized Large-Scale Graphene Platform with Large Chemical Enhancement in Surface-Enhanced Raman Scattering, ACS Nano. 5 (2011) 9799–9806. https://doi.org/10.1021/nn204156n.
[28] Y. Zhao, L. Xu, F. Kong, L. Yu, Design and preparation of poly(tannic acid) nanoparticles with intrinsic fluorescence: A sensitive detector of picric acid, Chemical Engineering Journal. 416 (2021) 129090. https://doi.org/10.1016/j.cej.2021.129090.
[29] S.E.J. Bell, N.M.S. Sirimuthu, Quantitative surface-enhanced Raman spectroscopy, Chem. Soc. Rev. 37 (2008) 1012. https://doi.org/10.1039/b705965p.
[30] Metal-phenolic networks as a versatile platform to engineer nanomaterials and biointerfaces - ScienceDirect, (n.d.). https://www.sciencedirect.com/science/article/pii/S1748013216304108 (accessed September 26, 2023).
[31] H. Geng, Q.-Z. Zhong, J. Li, Z. Lin, J. Cui, F. Caruso, J. Hao, Metal Ion-Directed Functional Metal–Phenolic Materials, Chem. Rev. 122 (2022) 11432–11473. https://doi.org/10.1021/acs.chemrev.1c01042.
[32] B. Lei, J.R. Bissonnette, Ú.E. Hogan, A.E. Bec, X. Feng, R.D.L. Smith, Customizable Machine-Learning Models for Rapid Microplastic Identification Using Raman Microscopy, Anal. Chem. 94 (2022) 17011–17019. https://doi.org/10.1021/acs.analchem.2c02451.
[33] C.-C. Qin, X.-P. Duan, L. Wang, L.-H. Zhang, M. Yu, R.-H. Dong, X. Yan, H.-W. He, Y.-Z. Long, Melt electrospinning of poly(lactic acid) and polycaprolactone microfibers by using a hand-operated Wimshurst generator, Nanoscale. 7 (2015) 16611–16615. https://doi.org/10.1039/C5NR05367F.
[34] L. Xie, K. Gong, Y. Liu, L. Zhang, Strategies and Challenges of Identifying Nanoplastics in Environment by Surface-Enhanced Raman Spectroscopy, Environ. Sci. Technol. 57 (2023) 25–43. https://doi.org/10.1021/acs.est.2c07416.
[35] Z. Wang, L. Huang, M. Zhang, Z. Li, L. Wang, H. Jin, X. Mu, Z. Dai, Chemical Mechanism-Dominated and Reporter-Tunable Surface-Enhanced Raman Scattering via Directional Supramolecular Assembly, J. Am. Chem. Soc. 144 (2022) 17330–17335. https://doi.org/10.1021/jacs.2c06026.
[36] L. Guerrini, E. Pazos, C. Penas, M.E. Vázquez, J.L. Mascareñas, R.A. Alvarez-Puebla, Highly Sensitive SERS Quantification of the Oncogenic Protein c-Jun in Cellular Extracts, J. Am. Chem. Soc. 135 (2013) 10314–10317. https://doi.org/10.1021/ja405120x.
[37] W. Lin, R. Jiang, S. Hu, X. Xiao, J. Wu, S. Wei, Y. Xiong, G. Ouyang, Investigating the toxicities of different functionalized polystyrene nanoplastics on Daphnia magna, Ecotoxicology and Environmental Safety. 180 (2019) 509–516. https://doi.org/10.1016/j.ecoenv.2019.05.036.

[38] L. Zhang, Z. Wang, N. Wang, L. Gu, Y. Sun, Y. Huang, Y. Chen, Z. Yang, Mixotrophic Ochromonas Addition Improves the Harmful Microcystis-Dominated Phytoplankton Community in In Situ Microcosms, Environ. Sci. Technol. 54 (2020) 4609–4620. https://doi.org/10.1021/acs.est.9b06438.
[39] G. Fan, P. Wasuwanich, M.R. Rodriguez-Otero, A.L. Furst, Protection of Anaerobic Microbes from Processing Stressors Using Metal–Phenolic Networks, J. Am. Chem. Soc. 144 (2022) 2438–2443. https://doi.org/10.1021/jacs.1c09018.
[40] J.A. Fuhrman, Marine viruses and their biogeochemical and ecological effects, Nature. 399 (1999) 541–548. https://doi.org/10.1038/21119.
[41] Q. Zhang, Y. Zhang, H. Chen, L. Zhang, P. Li, H. Xiao, W. Wu, One-dimensional nanohybrids based on cellulose nanocrystals and their SERS performance, Carbohydrate Polymers. 284 (2022) 119140. https://doi.org/10.1016/j.carbpol.2022.119140.
[42] J. Caldwell, P. Taladriz-Blanco, B. Rothen-Rutishauser, A. Petri-Fink, Detection of Sub-Micro- and Nanoplastic Particles on Gold Nanoparticle-Based Substrates through Surface-Enhanced Raman Scattering (SERS) Spectroscopy, Nanomaterials. 11 (2021) 1149. https://doi.org/10.3390/nano11051149.
[43] R. Yin, H. Ge, H. Chen, J. Du, Z. Sun, H. Tan, S. Wang, Sensitive and rapid detection of trace microplastics concentrated through Au-nanoparticle-decorated sponge on the basis of surface-enhanced Raman spectroscopy, Environmental Advances. 5 (2021) 100096. https://doi.org/10.1016/j.envadv.2021.100096.
[44] Q.T. Lê, N.H. Ly, M.-K. Kim, S.H. Lim, S.J. Son, K.-D. Zoh, S.-W. Joo, Nanostructured Raman substrates for the sensitive detection of submicrometer-sized plastic pollutants in water, Journal of Hazardous Materials. 402 (2021) 123499. https://doi.org/10.1016/j.jhazmat.2020.123499.
[45] Q. Yang, S. Zhang, J. Su, S. Li, X. Lv, J. Chen, Y. Lai, J. Zhan, Identification of Trace Polystyrene Nanoplastics Down to 50 nm by the Hyphenated Method of Filtration and Surface-Enhanced Raman Spectroscopy Based on Silver Nanowire Membranes, Environ. Sci. Technol. 56 (2022) 10818–10828. https://doi.org/10.1021/acs.est.2c02584.
[46] L. Chang, S. Jiang, J. Luo, J. Zhang, X. Liu, C.-Y. Lee, W. Zhang, Nanowell-enhanced Raman spectroscopy enables the visualization and quantification of nanoplastics in the environment, Environ. Sci.: Nano. 9 (2022) 542–553. https://doi.org/10.1039/D1EN00945A.
[47] R. Hu, K. Zhang, W. Wang, L. Wei, Y. Lai, Quantitative and sensitive analysis of polystyrene nanoplastics down to 50 nm by surface-enhanced Raman spectroscopy in water, Journal of Hazardous Materials. 429 (2022) 128388. https://doi.org/10.1016/j.jhazmat.2022.128388.

607

Table of Contents

608